Hindawi
Advances in Civil Engineering
Volume 2019, Article ID 5129274, 13 pages
https://doi.org/10.1155/2019/5129274

Research Article

A Predictive Model for Damage Assessment and Deformation in Blast Walls Resulted by Hydrocarbon Explosions

Majid Aleyaasin

Lecturer School of Engineering, University of Aberdeen, Aberdeen AB24 3UE, UK

Correspondence should be addressed to Majid Aleyaasin; eng780@abdn.ac.uk

Received 18 February 2019; Revised 7 May 2019; Accepted 10 June 2019; Published 4 July 2019

Academic Editor: Chiara Bedon

In this paper, a new method is developed to find the ductility ratio in blast walls, resulted by hydrocarbon explosions. In this method, only the explosion energy and distance from the centre of explosion are required to find the damage by using simple predictive models in terms of empirical-type formulas. The explosion model herein is a TNO multiphysic method. This provides the maximum overpressure and pulse duration in terms of the explosion length and distance from explosion centre. Thereafter, the obtained results are combined with the SDOF model of the blast wall to determine the ductility ratio and the damage. By using advanced optimisation techniques, two types of predictive models are found. In the first model, the formula is found in terms of 2 parameters of explosion length and distance from explosion centre. However, the 2nd model has 3 parameters of explosion length, distance, and also the natural period of the blast wall. These predictive models are then used to find explosion damages and ductility ratio. The results are compared with FEM analysis and pressure-impulse (P-I) method. It is shown that both types of models fit well with the outputs of the simulation. Moreover, results of both models are close to FEM analysis. The comparison tables provided in this paper show that, in the asymptotic region of P-I diagrams, results are not accurate. Therefore, this new method is superior to classical pressure-impulse (P-I) diagrams in the literature. Advantage of the new method is the easy damage assessment by using simple empirical-type formulas. Therefore, the researchers can use the method in this paper, for damage assessment in other types of blast resistive structures.

1. Introduction

Blast walls are sacrificial barriers to protect offshore structures when subjected to hydrocarbon explosions. Substantial research has been performed to develop a code of practice for design of such structures [1]. The theoretical foundations for designing blast-resistive structures and blast walls can be found in [2, 3].

An analytical method based on plate theory for blast wall design [4] is rarely used in the literature since the results of those studies cannot be used directly as a design code. However, linear and nonlinear finite elements have been used significantly (for example, [5, 6]). They are applicable in cases where batch simulations enable cost-benefit analysis [7].

Presently, the dominant approach is a single degree Of freedom (SDOF) method [1–3] and leads to some design curves known as Bigg's chart. They appeared first in a well-known book [8] but originated from the initial attempt by Newmark [9]. This SDOF method enables the famous pressure-impulse (P-I) diagrams which was first introduced in [9] to be constructed [1–3].

These P-I diagrams strongly depend on pressure versus time expression (pulse shape) of the explosion [10], and together with SDOF modelling, they are used to find the blast response of complex of structures, such as cable-supported facades [11]. Both SDOF-type model [12] and continuous beam model [13] are used for developing P-I diagrams. Recently, it is shown that batch finite element simulations [14] cannot lead to P-I diagram unless preliminary information regarding SDOF parameters is available.

Regardless of importance of the P-I diagrams in the damage assessment, they are not straightforward and the designer needs substantial information about the calculation of the explosive loads and pulse shape to be able to use P-I

diagrams in damage assessment. There is not any attempt (or new method) that directly connects intensity of explosion to the resulted damage and deflection in the blast walls. Recently, the author looked at this important issue where, in the vicinity of box girders [15], TNT explosions may occur. Since the possibility of hydrocarbon explosions are much higher than any terrorist activities, blast walls are used in many offshore structures. Therefore, any research regarding this topic is justifiable.

In this article, the explosive physics known as the multienergy method known as TNO [16], and further models fitted into it [17], is combined with the SDOF method for deformation of the blast walls. Thereafter, the deformation and ductility, for both rigid plastic models and elastic-plastic models, are determined in each distance and explosion length. Then outcomes of the batch simulations are exported to advanced optimisation programs to develop two types of predictive models expressed by using simple empirical-type formulas.

Using any of the models in this paper, the designer can find the deformation (or ductility) from the intensity of explosions (explosion length), distance of the blast wall from explosion centre, and natural period of the blast wall. As far as the author is aware, this new method is the easiest one for predicting the damage in the blast wall, thereby declaring the explosion resistance. The knowledge about explosion physics is embedded in the formulas. Therefore, it is an excellent tool for preliminary analysis of the blast wall.

In a case study, in the asymptotic region of the P-I diagram, it is shown that, while P-I provides inaccurate results, this method leads to accurate results, when it is compared with FEM simulation of the blast wall. Therefore, the approach herein can be extended to other types of structures in future to replace P-I diagrams (or FEM) for predicting the damage.

2. Overpressure History in Explosions

When hydrocarbon mass m_c (in kg) with heat energy ΔH_c (Joule/kg) causes an explosion with efficiency η, the resulted explosive energy E_0 will be

$$E_0 = \eta m_c \Delta H_c. \tag{1}$$

In the TNO multienergy method [16], an explosion length is defined by

$$R_0 = \left(\frac{E_0}{p_0}\right)^{1/3}, \tag{2a}$$

where p_0 is the atmospheric pressure (in Pa); therefore, R_0 truly has units of the length (m). If R_s is the distance from the explosion centre (m), dimensionless $\overline{R}$ will be defined by

$$\overline{R} = \frac{R_s}{R_0} = \left(\frac{E_0}{p_0}\right)^{-1/3} R_s. \tag{2b}$$

Then, the overpressure p_{max} (in bar, i.e., dimensionless) and explosion pulse duration $\overline{t}_+$ (dimensionless) can be found from TNO charts [16]. In those charts, the overpressure and duration can be found from the curves designated by the level of the explosion. The charts are developed from computer simulations performed in eighties and are strongly applicable to hydrocarbon explosions. Due to the importance of the TNO charts, researchers produced curve fitted formulas for the data in those charts. These formulas are given in [17] via the following equation:

$$\begin{aligned}
&0.6 \le \overline{R} \le 30 \quad p_{max} = 0.0605\overline{R}^{-0.99} \quad p_{max}\overline{t}_+ = 0.0605\overline{R}^{-0.99} \quad \text{Level 3},\\
&0.6 \le \overline{R} \le 100 \quad p_{max} = 0.301\overline{R}^{-1.11} \quad p_{max}\overline{t}_+ = 0.114\overline{R}^{-1.03} \quad \text{Level 6},\\
&2 \le \overline{R} \le 100 \quad p_{max} = 0.318\overline{R}^{-1.13} \quad p_{max}\overline{t}_+ = 0.114\overline{R}^{-1.03} \quad \text{Level 9}.
\end{aligned} \tag{3}$$

It should be reminded that another valuable software is provided for blast waves (for example, [18, 19]) but not reformulated for designers yet (such as (3)). In the above expressions, $\overline{t}_+$ is dimensionless overpressure pulse duration given in [16]:

$$\overline{t}_+ = \frac{t_d C_0}{R_0}, \tag{4}$$

where t_d is the overpressure duration in sec and C_0 is the sound velocity at atmospheric conditions in m/sec. Majority of explosions will fall into all of the three levels in (3). It is recommended that the overpressure and duration should be computed in each level and the average value should be taken into consideration [17].

The author herein produced the overpressure contours in terms of R_0 and R_s which are two important parameters in any explosions. They are shown in Figure 1 and are used in the next part of the paper, for developing the new method.

3. SDOF Model for Blast Walls

The typical geometry of the cross section of a blast wall [1] is similar to (a) in Figure 2.

The finite element analysis shows [5] the deformation pattern resulted by an explosion by using shell elements which is similar to Figure 3.

The front view of a typical blast wall [1] is shown in (b) in Figure 2. The main parameter is the pitch $\overline{p}$ that is shown in (a). The wall is connected to the structure by upper and lower supports shown in (c). When overpressure p_{max} is applied to the wall with uniform distribution, the upper and lower supports with thicknesses t_U and t_L (in m) (see (c) in Figure 2) have equivalent lengths L_U and L_L shown in (Figure 15). They will yield since they have limited yield stress f_y^* (Pa). The total length is L (in m), and $(M_{c,Rd})_U$ and $(M_{c,Rd})_L$ are the yield moments (per length, i.e., in N) of the upper and lower supports and are given by the following equations [1–3]:

$$\begin{aligned}
\left(M_{c,Rd}\right)_U &= \frac{t_U^2 f_y^*}{4},\\
\left(M_{c,Rd}\right)_L &= \frac{t_L^2 f_y^*}{4}.
\end{aligned} \tag{5}$$

$M_{c,Rd}$ or the plastic bending moment (per unit length) of the main wall is given by (6). It depends on the details of the

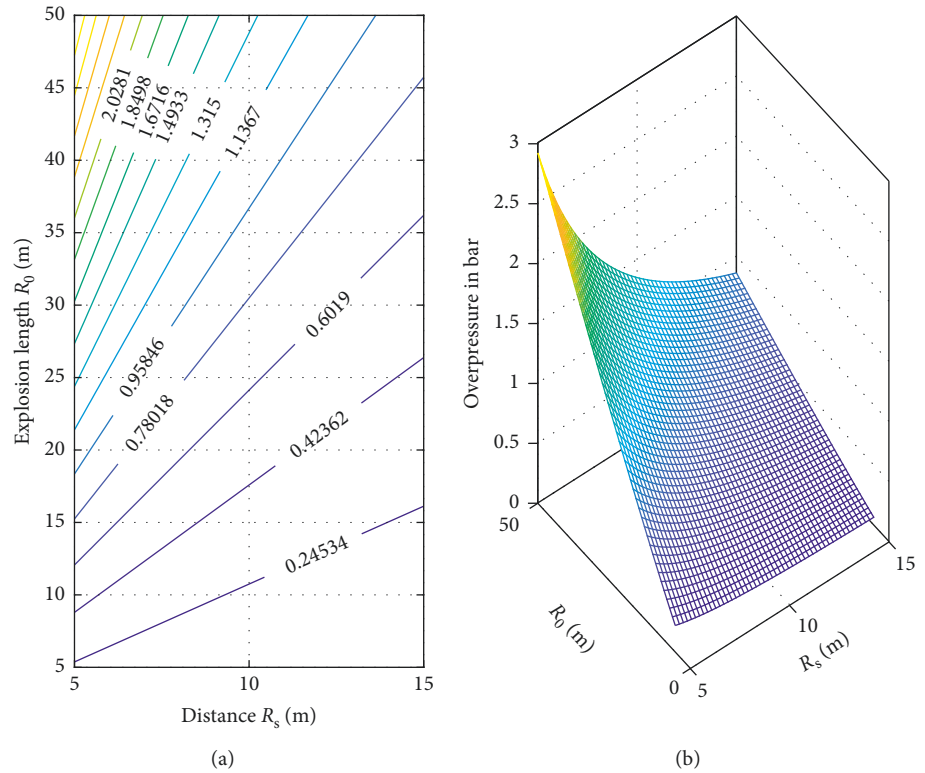

(a) (b)

Figure 1: Overpressure in the TNO model for explosion. (a) Overpressure contours in bar. (b) Average value of levels 3, 6, and 9.

cross section in (a) in Figure 2, which are designated by two parameters, $W_{pl,y}$ (plastic section modulus) and f_y^* (material yield stress) of the cross section:

$$M_{c,Rd} = \frac{W_{pl,y} f_y^* K_F K_{VM}}{\overline{p}}. \tag{6}$$

K_F and K_{VM} in (6) are flattening and shear correction factors described in [1]. The equivalent length of the blast wall L_E is less than the total length L and can be found by

$$L_E = \frac{2L}{\sqrt{1+\left(\left(M_{c,Rd}\right)_L / M_{c,Rd}\right)} + \sqrt{1+\left(\left(M_{c,Rd}\right)_U / M_{c,Rd}\right)}}. \tag{7}$$

Derivation of (7) is shown in Appendix A, and instead of total length, L_E will be used in all calculations, regarding the blast wall. For example, the stiffness per unit length will be given as shown in [1–3] as follows:

$$k = \frac{384EI}{5L_E^3 \overline{p}}. \tag{8}$$

The corrected stiffness of wall k_R is recommended in [1] to correct (8) resulted from beam theory which is

$$k_R = \frac{kL_E}{1.6L - 0.6L_E}. \tag{9}$$

Equations (8), (9), and others that follow are true when the SDOF method is chosen as a route of the analysis, where the beam simplification and can be justified. This is also current practice for the preliminary design of blast walls [1–3]. However, for the detail of the buckling pattern similar to Figure 3, the beam model simplification is not appropriate. According to rigid plastic theory in structures, the maximum resistance of a beam cross section R_m [2, 3] is given by

$$R_m = \frac{8M_{c,Rd}}{L_E}. \tag{10}$$

This R_m is defined for finding maximum elastic deformation of the wall y_{el} [1–3] by using the following formula:

$$y_{el} = \frac{8M_{c,Rd}}{k_R L_E}. \tag{11}$$

However, if the maximum blast load F_1 given by the following equation exceeds R_m, the wall deforms plastically:

$$F_1 = A_s p_{max}. \tag{12}$$

In (12), A_s is the projected blast area per pitch in Figure 4. For further clarification, this area with the pressure p_{max} applied to it is shown in Figure 4.

The deformation is allowed up to the ductility limit. The ductility μ is very important in design of structures under extreme and blast loading [2, 3, 8] and is the ratio of maximum plastic deformation to the elastic limit y_{el} given by

$$\mu = \frac{y_{max}}{y_{el}}. \tag{13}$$

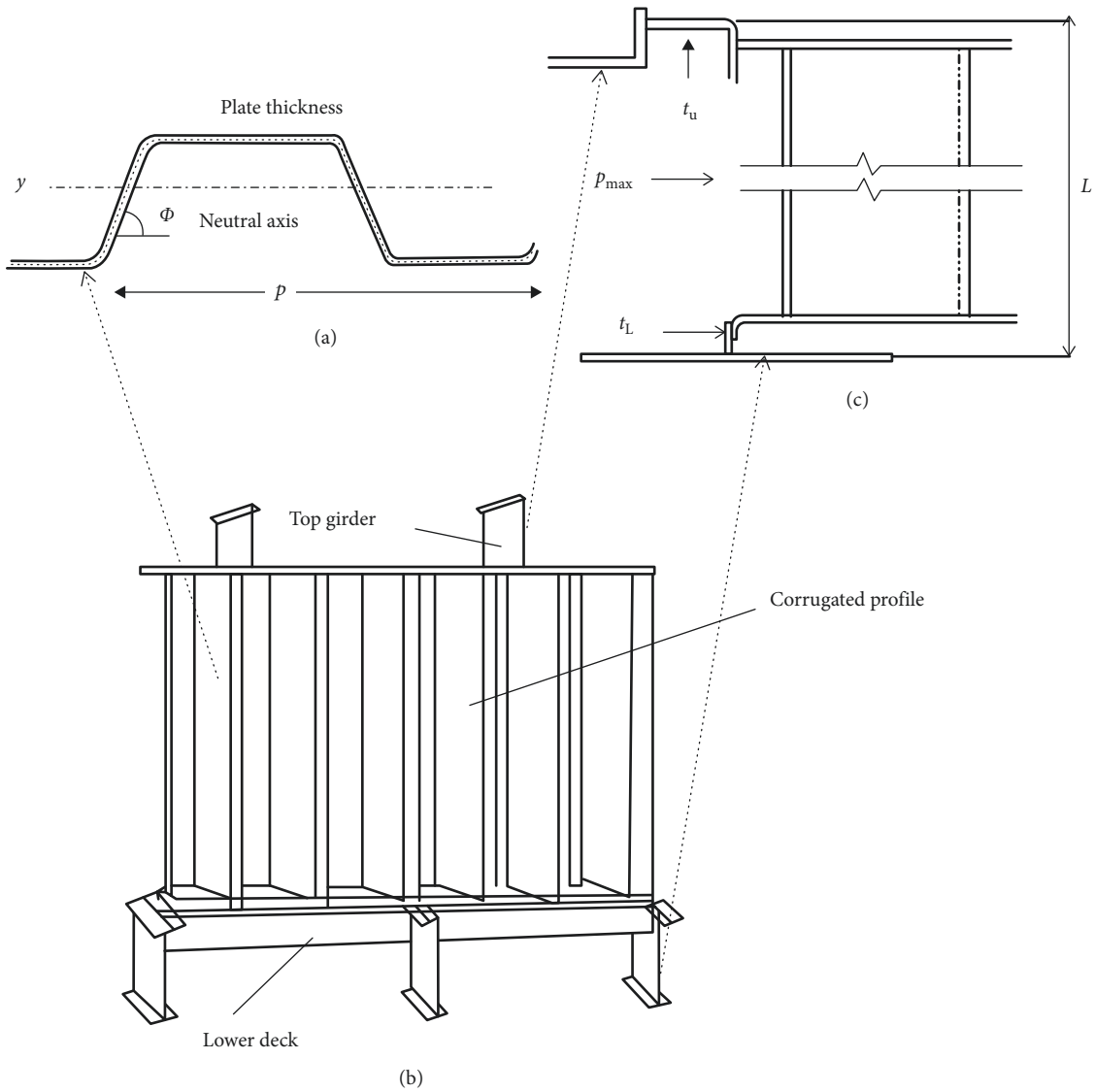

Figure 2: (a) Cross section of the (b) blast wall (front view) and (c) upper and lower supports.

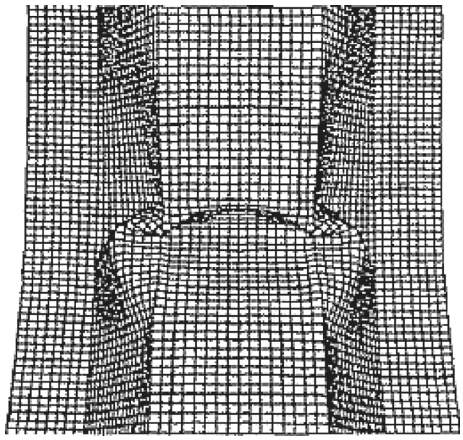

Figure 3: Deformation pattern from FEM analysis.

The backbone of the SDOF model relies on the natural period of free structural vibration T, [2, 3, 8] of the blast wall which will be given by

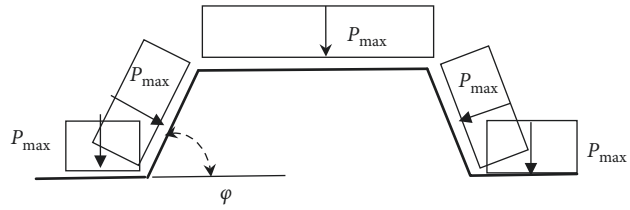

Figure 4: Applied pressure on the wall surface.

$$T = 2\pi\sqrt{\frac{MK_{LM}}{\overline{p}k_R}}. \tag{14}$$

In (14), M is the blast wall mass (for one pitch) and K_{LM} is the correction factor for the distributed mass. In Appendix B, it shows that for rigid plastic theory based on plastic hinge assumption [2, 3], we find that $K_{LM} = 0.333$. However, in the current practice [1], designers use higher values without any justification. Part of this article

investigates how this apparent inconsistency can affect the ductility results.

The SDOF modelling is well known by Biggs' chart since it appeared in a famous book [8]. However, the initial research is done by Newmark who is one of the pioneers in structural dynamic. He summarised Bigg's chart a decade before it is seen in [8], in his famous paper [9] by using the following formula:

$$\frac{F_1}{R_m} \cong \frac{\sqrt{2\mu - 1}}{(t_d/T)\pi} + \frac{(1-(1/2\mu))(t_d/T)}{(t_d/T)+0.7}. \quad (15)$$

All the parameters in (15) are described in previous formulas. When an explosion with length R_0 occurs at distance R_s, one can find the preliminary ductility curves. For a particular blast wall that is designed by a manufacturer, geometrical and material details are available. Therefore, the ductility contour can be constructed easily from (15), without using the pressure-impulse diagram of the blast wall.

4. Numerical Example

For a steel blast wall with pitch $\overline{p} = 1.2$ meter, the cross-sectional dimensions are shown in Figure 5. It is one of the existing profiles of the blast wall that is described in [1].

The second moment of the cross section $I = 8.767 \times 10^{-5}\,\mathrm{m}^4$, the section modulus $W_{pl,y} = 4.37\times 10^{-4}\,\mathrm{m}^3$, mass per pitch $M = 410\,\mathrm{kg}$, thicknesses of the upper and lower supports $t_U = 12\,\mathrm{mm}$ and $t_L = 10\,\mathrm{mm}$, and Young's modulus $E = 210\,\mathrm{GPa}$, and yield stress $f_y^* = 400\,\mathrm{MPa}$, the length $L = 3\,\mathrm{m}$, and the correction factors [1] $K_F = 0.9$ and $K_{VM} = 0.95$. In Figure 6, the ductility is shown, which is the result of substantial simulations of the SDOF model for this blast wall.

Figure 6 is prepared for $K_{LM} = 0.85$ as recommended in [1] and is not the result of rigid plastic theory. Figure 6 is drawn in range $15 < R_0 < 25$ and $5 < R_s < 10$, and the contours seem linear and visible. However, for higher ranges, visibility and linearity cannot be observed.

5. Model with Two Parameters

A nonlinear predictive model of Figure 6 with two parameters R_0 and R_s (both explosion related) can be suggested in this form:

$$\mu \cong C_{\mu 2} R_0^{\alpha} R_s^{\beta}. \quad (16)$$

For example, the higher range estimation of ductility for can be replaced by the following approximate expression:

$$\mu \cong 1.0008 R_0^{4.2434} R_s^{-6.2520}, \quad 20 < R_0 < 50,\ 10 < R_s < 15. \quad (17)$$

In Figure 7, the computed ductility ratio and the estimated ductility ratio in (17) are drawn together. It can be concluded that, in higher ductility ratios, where severe plastic deformation occurs, the estimated ductility is very close to the computed ductility. In (17), only explosion-related parameters are used. Three parameter models will be discussed as well.

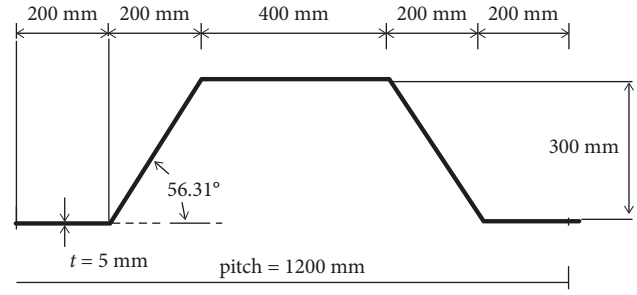

Figure 5: A typical cross section (one pitch) of a blast wall [1].

6. Rigid Plastic Modelling

Rigid plastic theory [2, 3] assumes plastic hinge at the midlength of the blast wall. In appendix B, it is shown that, in such situation, the equivalent mass $M_e = M/3$ and $K_{LM} = 0.333$. The damage calculation will be straightforward because the calculations regarding overpressure and duration remain the same as the ones used for producing Figure 7. Obviously if we assume $K_{LM} = 0.333$, the results will change which is shown in Figure 8. The region in which ductility ratio is below 1 remains elastic, and by producing such contour maps, the pressure-impulse diagram is not required. If we compare Figure 6 in which peak deformation $y_{max} = 3.75 y_{el}$ with Figure 8 in which $y_{max} = 5.03 y_{el}$, we can conclude that considering $K_{LM} = 0.333$ (rigid plastic model) provides conservative estimation for ductility.

7. Model with Three Parameters

A nonlinear predictive model with three parameters R_0, R_s (explosion related), and T in (14) which are blast wall related can be suggested as in the following form:

$$\mu \cong C_{\mu 3} R_0^{\alpha} R_s^{\beta} T^{\gamma}. \quad (18)$$

The parameters $C_{\mu 3}, \alpha, \beta$, and γ in (18) can be found by taking the logarithm for that expression that will change it into

$$\log(\mu) \cong \log\left(C_{\mu 3}\right) + \alpha \log(R_0) + \beta \log(R_s) + \gamma \log(T). \quad (19)$$

The above expression enables the linear regression techniques to be implemented for finding the parameters $C_{\mu 3}, \alpha, \beta$, and γ. These parameters can be found by using nonlinear regression analysis. Moreover, the powerful Nelder–Mead algorithm [20] which is built in MATLAB is also used, to find the fractional powers α, β, and γ in (18). Finally, the numerical expression of (18) when $K_{LM} = 0.333$ (rigid plastic modelling) will be in the following form:

$$\mu \cong 1.0008 R_0^{4.4483} R_s^{-6.1082} T^{.02698}, \quad 20 < R_0 < 50,\ 10 < R_s < 15. \quad (20)$$

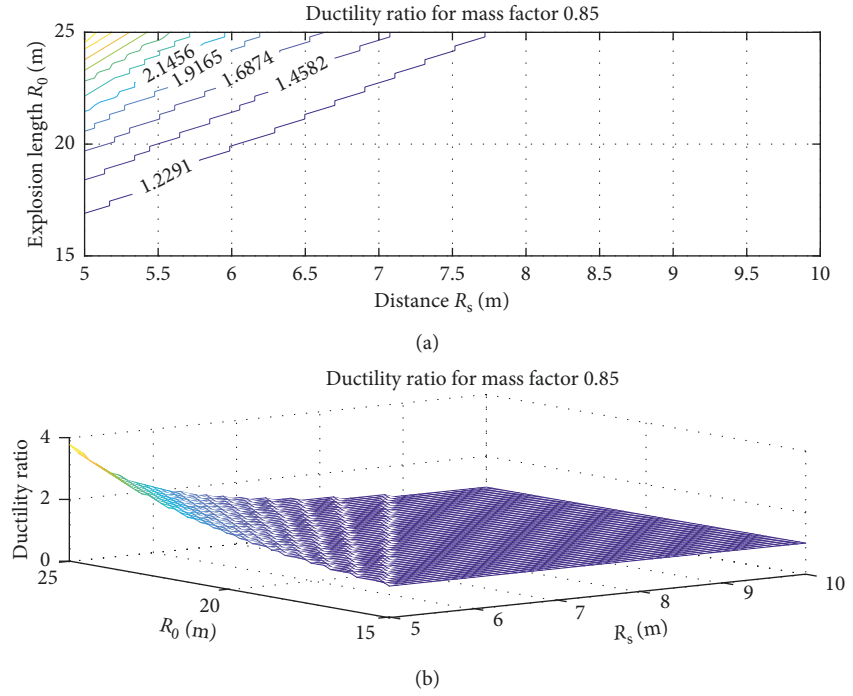

Figure 6: Contours for the ductility ratio.

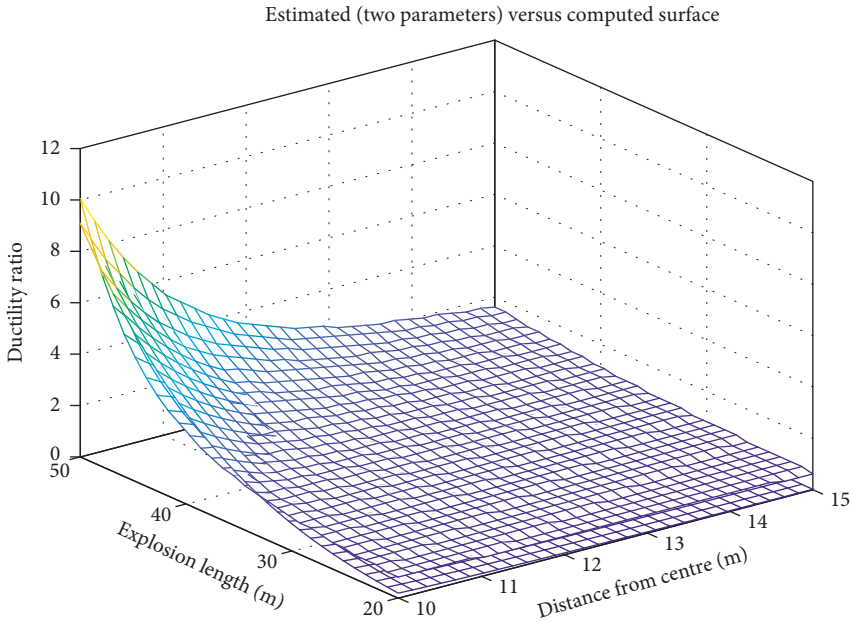

Figure 7: Computed versus estimated ductility ratio.

In Figure 9, the computed ductility ratio and the estimated ductility ratio in (20) are drawn together. It can be concluded that, in higher ductility ratios, where severe plastic deformation occurs, the estimated ductility is very close to the computed ductility. In (20), explosion-related parameters plus blast wall natural period are used. Three-parameter models use $K_{LM} = 0.333$ (rigid plastic modelling) because of its conservativeness in estimation of the maximum ductility.

The author has suggested many other forms for the regression analysis, using advanced optimisation techniques [20], and so far, he has not found better forms than (20) for the 3-parameter-type model and (17) for the 2-parameter-type model. It is quite possible that some other forms with closest fit may be found by further research.

8. Comparison of the Results

Consider that an explosion with effective energy $E_0 = 9500$ MJ occurs at distance $R_s = 12$ m from the explosion centre. According to parameters (2a), (2b) and (3).

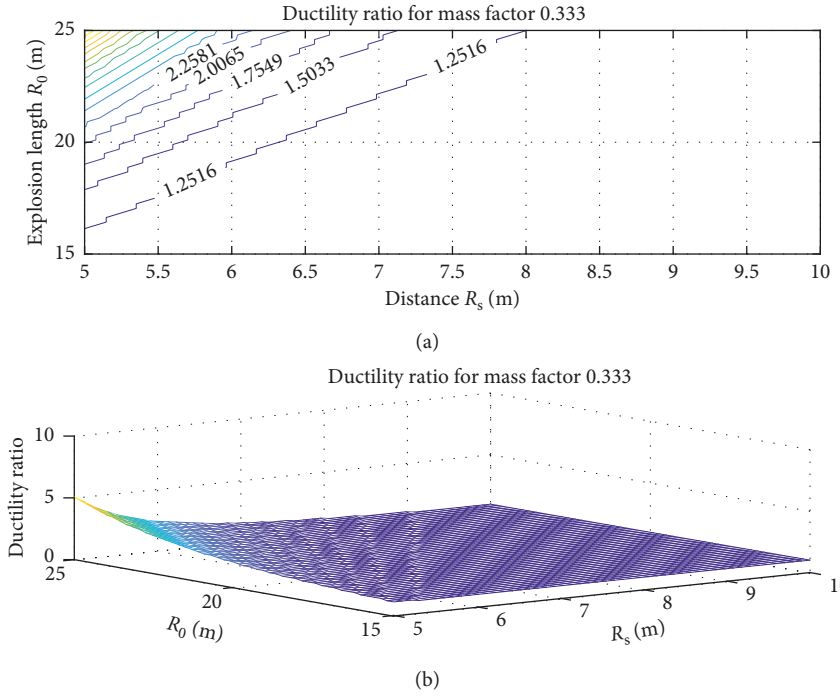

Figure 8: Contours for the ductility ratio in the rigid plastic model.

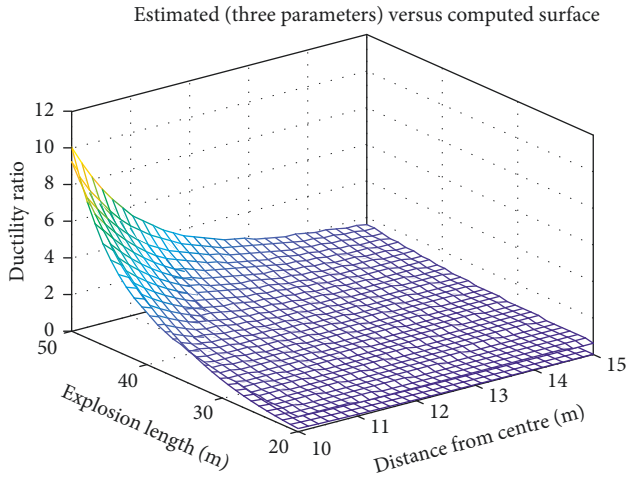

Figure 9: Computed versus estimated ductility ratio.

The overpressure is the average value of the explosion levels 3 and 9 and 6, in (3).

$$\begin{aligned} R_0 &= 45.629\,\text{m}, \\ \overline{R} &= 0.263, \\ p_{\max} &= 0997\,\text{bar}. \end{aligned} \tag{21}$$

The elastic deformation from (11) is $y_{\text{el}} = 7.8\,\text{mm}$, whereas the maximum deflection at the middle section, $y_{\max}$, in (12) can be found by knowing about the ductility ratio.

Since the velocity of sound in the room temperature condition is $C_0 = 340\,\text{m/sec}$, from formula (4), we have duration of the explosion pulse $t_{\text{d}} = 74\,\text{msec}$, whereas the natural period of the blast wall herein which is given by using (14) is $T = 16.1\,\text{msec}$.

The pressure-impulse curve that introduced before is still used for damage assessment for many structures. They are a series of the asymptotic curves inscribed in the vertical and horizontal asymptotes. To find the points on the curves, either we use analytical methods [21, 22] or numerical methods [23] and sometimes FEM analysis [24]. In the x-y plane, the vertical axis displays $F_{\max}/K_{\text{e}}y_{\text{el}}$, whereas horizontal axis displays $x = I/y_{\text{el}}\sqrt{K_{\text{e}}M_{\text{e}}}$, I is the impulse, and $F_{\max}$ is the maximum explosion forces. With uniform overpressure, they are

$$\begin{aligned} F_{\max} &= A_{\text{eff}}p_{\max}, \\ I &= 0.5F_{\max}t_{\text{d}}. \end{aligned} \tag{22}$$

In [2, 3], it can be shown that the equations of the vertical and horizontal asymptotes are in terms of the ductility ratio μ that is defined in (13), i.e.,

$$\begin{aligned} \frac{I}{y_{\text{el}}\sqrt{K_{\text{e}}M_{\text{e}}}} &= \sqrt{2\mu - 1}, \\ \frac{F_{\max}}{K_{\text{e}}y_{\text{el}}} &= \frac{2\mu - 1}{2\mu}. \end{aligned} \tag{23}$$

Typical curves for elastic-plastic structures are shown in Figure 10 in which the ductility ratio can be found via interpolation. The snapshot designated by the point shows the coordinates $I/y_{\text{el}}\sqrt{K_{\text{e}}M_{\text{e}}} = 13.622$ and $F_{\max}/K_{\text{e}}y_{\text{el}} = 1.03$ that correspond to this particular explosion, and we can find the ductility $\mu \cong 7.24$ as a result of this explosion.

However, the direct simulation in this paper shows that $\mu \cong 2.414$. It shows that the P-I method particularly in asymptotic ends are significantly inaccurate. The two

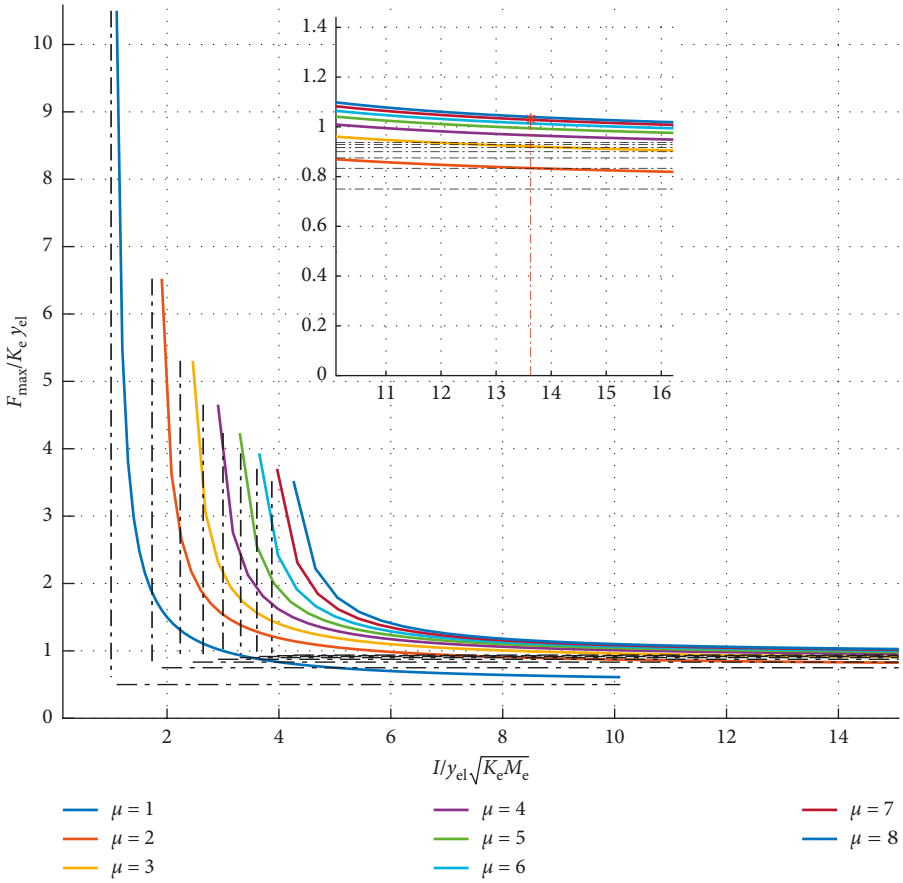

Figure 10: Pressure-impulse diagram for elastic-plastic structures.

approximated models in this paper that are expressed by (17) and (20) to replace the P-I method give much closer results. The comparison is shown in Table 1.

Further comparison can be done by using FEM technique via ABAQUS modelling [25] of the blast wall in this example. The meshing is shown by a snapshot in Figure 11. In this model 6500-shell-type S4R elements, each with nine internal integration point are used. Obviously substantial FEM outputs, including the local buckling details in bottom flanges are available. However, the one that can be compared with y_{max} in (12) has been extracted. Since ductility ratio is not defined in ABAQUS, Table 2 is provided to compare the y_{max} (maximum deflection) in each approach.

The last row of Table 2 is found from history of the displacement of the middle of the top flange of the blast wall. This history for U, V, and A is shown in Figure 12. It is obvious that velocity in mm/s and acceleration in m/s^2 are big numbers since T in (14) is very low.

Figure 12 is prepared by using history of nodes. However, the history of stress and strain in any location of the blast wall can be prepared by element output files. Similar to Figure 11, Figure 13 shows the Mises stress map that is scaled in Pa.

Obviously, the yield stress is $f_y^* = 400$ MPa, and the material is assumed elastic-perfectly plastic (E-P-P); all similar to the SDOF model. Since the blast wall is modelled with shell elements, Poisson's ratio of the material $\upsilon = 0.3$ is also required. The history of the Mises stress and also the maximum principal strain can be found from the element file. To do this, the shell element corresponding to middle of the top flange of the blast wall is chosen. The history file for stress and stain for that location is shown in Figure 14. It is obvious that stress does not exceed 400 MPa. However, for strain after quick jump at the beginning of the explosion, the fluctuations are not significant. From the model in this paper, we can check and verify the displacement as shown in Table 2. This suits the purpose of this paper in developing a simple and accurate model for checking high-fidelity FEM analysis.

In Table 3, the material properties and also maximum velocity, acceleration, and stress and strain are shown. The maximum displacement is shown in Table 2 for the comparison purposes. The maximum stress in Table 3 exceeded slightly above 400 MPa because the E-P-P material model is ABAQUS, which is expressed via a very low plastic Young's modulus (not zero).

Table 1: Comparison of the results (ductility ratio).

The method used	Ductility ratio
TNO + SDOF simulation	$\mu \cong 2.414$
Pressure-impulse curves	$\mu \cong 7.24$
Two-parameter empirical formula (17)	$\mu \cong 1.968$
Three-parameter empirical formula (20)	$\mu \cong 2.019$

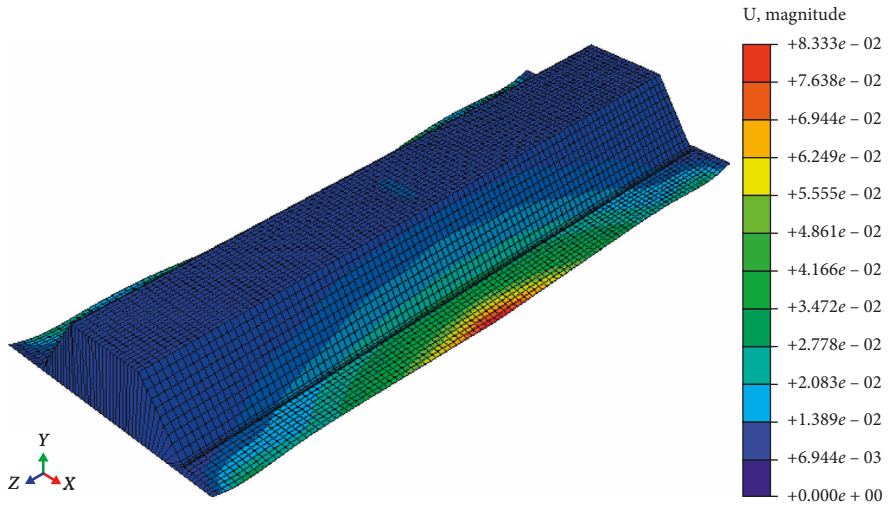

Figure 11: FEM meshing of the blast wall (displacement map in m).

Table 2: Comparison of the results (maximum deflection).

The method used	Maximum deflection
TNO + SDOF simulation	$y_{max} \cong 18.9$ mm
Pressure-impulse curves	$y_{max} \cong 56.7$ mm
Empirical formula (17)	$y_{max} \cong 13.2$ mm
Empirical formula (20)	$y_{max} \cong 15.8$ mm
FEM analysis via ABAQUS	$y_{max} \cong 19.5$ mm

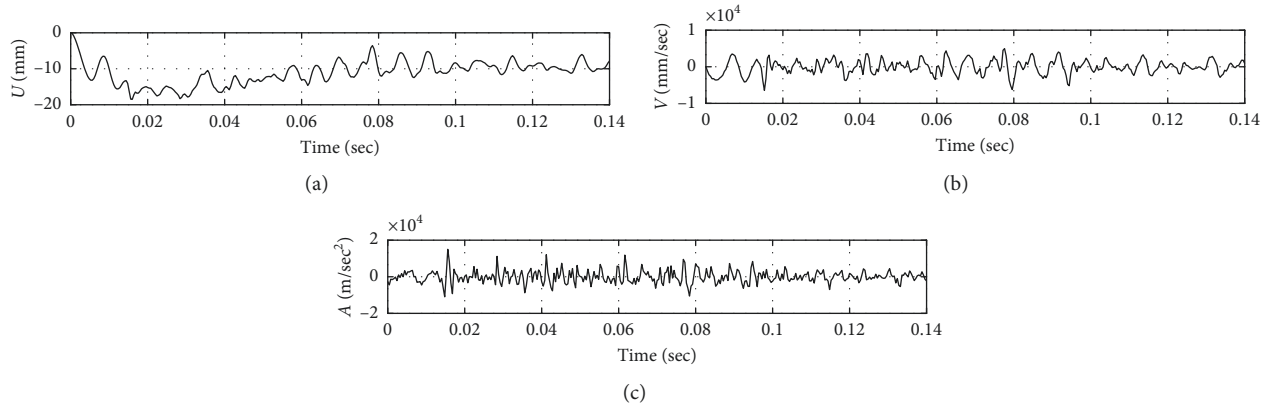

Figure 12: (a) Displacement (deflection), (b) velocity, and (c) acceleration history of the top flange.

The outcomes of this section are shown in Table 4. This table compares the advantages and disadvantage of each method that is discussed. It can be seen that there are many advantages of using the method in this paper, particularly when we compare with the pressure-impulse diagram. However, it should be used together with high-fidelity FEM analysis to achieve more details about the response of the blast wall to the explosion.

9. Conclusions and Remarks

It this paper, a new method for damage assessments in blast walls are developed. It is much easier than the classical method of the pressure-impulse diagram and FEM analysis. As shown in [21–24], and also in this paper, the high-fidelity analytical or FEM models cannot predict explosion response without knowledge about explosion overpressure and pulse duration.

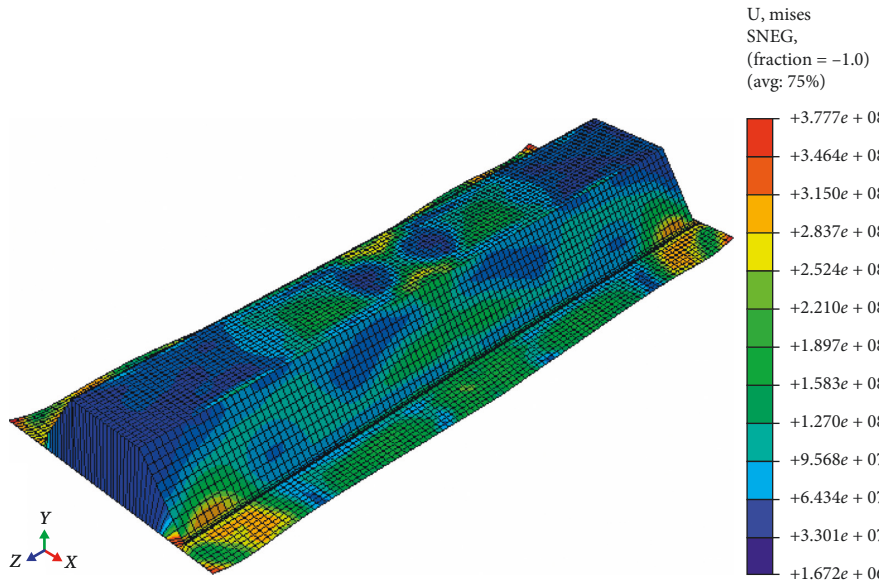

Figure 13: Mises stress map scaled in Pa.

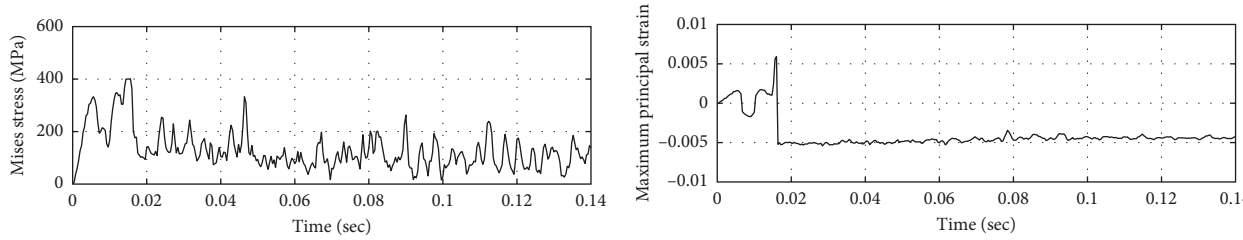

Figure 14: History of (a) Mises stress and (b) maximum plastic strain of the middle of top flange.

Table 3: Summary of FEM analysis (results are for middle of the top flange).

Young's modulus for E-P-P steel	$E = 210\,\text{GPa}$
Poisson's ratio	$\upsilon = 0.3$
Maximum velocity	$v_{\max} = 6456\,\text{mm/s}$
Maximum acceleration	$a_{\max} \cong 15001\,\text{m/s}^2$
Maximum Mises stress	$\sigma_{\max} \cong 400810000\,\text{Pa}$
Maximum principal strain	$\varepsilon_p = 00059$

Table 4: Comparison table for methods discussed.

The method used	Advantages	Disadvantages
TNO + SDOF simulation	(1) Reliable source for checking FEM (deflection) (2) Simple compared to FEM	(1) Low fidelity compared to FEM analysis (2) Includes the model for history of overpressure
Pressure-impulse curves	(1) Simple to find the ductility and displacement	(1) Inaccuracy in asymptotic region (2) Needs overpressure history (3) Low fidelity compared to FEM analysis
Empirical formulas (17) and (20) in this paper	(1) No need for history of overpressure (2) Simple to find the ductility and displacement (3) Reliable source for checking FEM (deflection)	(1) Low fidelity compared to FEM analysis
FEM analysis via ABAQUS	(1) High fidelity of the model (2) Availability of results in any location (3) Local buckling details	(1) Needs overpressure history (2) Meshing difficulties and model complexity (3) Verification of the results by another method

The inaccuracy of the P-I diagram in the asymptotic region is clearly shown in this paper via Tables 1 and 2. Regardless of that, the P-I diagram is an active field of research for blast-resistive structure as seen in recent publications [22–24]. Therefore, an alternative method is required to replace the P-I diagram in asymptotic region. This approach

should be much easier than FEM analysis and can produce a result accurate enough to be compared with FEM. The author believes that he has found an alternative in this paper.

When overpressure-time history is not available, both of the SDOF and FEM cannot predict the damage. The advantage of this new method is the combination of SDOF method and overpressure-time history of explosion. Herein the TNO method (that provides overpressure history) with SDOF (that provides deflection) has been combined together. Thereafter approximate formulas have been produced that easily predicts the ductility ratio without using P-I diagrams or doing SDOF calculations or FEM analysis. Therefore, it will be very useful for preliminary design applications.

Symbols

A_s: Cross-sectional area
A, B, C: Constants of the parabolic function
A_{eff}: Effective overpressured area
C_0: Velocity of sound
E_0, E: Explosive energy and modulus of elasticity
f_y^*, F_1: Steel yield stress and total applied force
F_{max}: The maximum explosion force
I: Second moment of cross section (in bending)
I: Impulse of the explosion pulse
k, k_R: Stiffness and reduced stiffness (in bending)
K_F, K_{VM}: Flattening and shear correction factors
K_{LM}: Mass correction factor
L, L_E: Total length and equivalent length
L_U, L_L: Lengths of the upper and lower supports
M, M_e: Mass and equivalent mass of the blast wall
m_c: Hydrocarbon mass
$(M_{c,Rd})_U$, $(M_{c,Rd})_L$: Yield bending moment in the upper and lower supports
$M_{c,Rd}$: Yield bending moment in the blast wall
p_{max}: Maximum overpressure
$\overline{p}$, p_0: Projected blast area per pitch and atmospheric pressure
R_0, $\overline{R}$: Explosion length and dimensionless explosion length
R_m: Maximum elastic resistance of beam cross section
R_s: Distance from explosion centre
$\overline{t}_+$, t_d: Dimensionless pulse duration and pulse duration
t_U and t_L: Thicknesses of the upper and lower supports
T: Natural period of the structure
$W_{pl,y}$: Plastic section modulus
W_0: Maximum deflection of the midspan
y_{el}, y_{max}: Maximum elastic and maximum plastic deformation
ΔH_c: Heat energy
α, β, γ: Constants in the predictive model
μ: Ductility ratio
η: Efficiency of explosion.

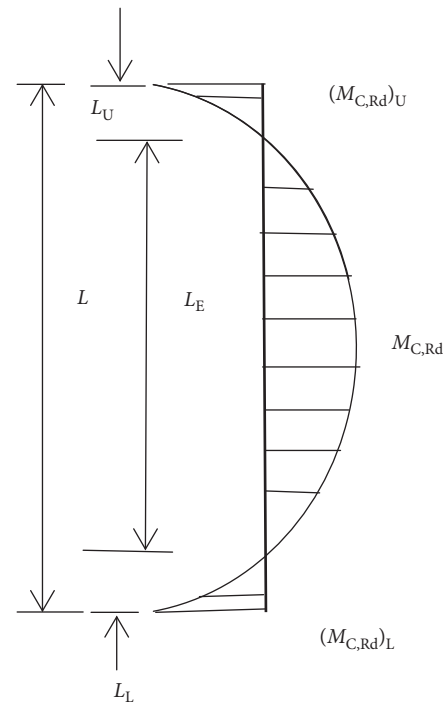

Figure 15: Parabolic bending moment distribution.

Appendix

A. Equivalent Lengths and Bending Moment Distribution

According to Figure 15, the total length of the blast wall consist of 3 parts:

$$L = L_E + L_U + L_L. \tag{A.1}$$

The overpressure as a result of explosion produces a uniform load that results a parabolic type of bending moment as follows:

$$M(x) = Ax^2 + Bx + C. \tag{A.2}$$

When we place the origin of the coordinate system at the middle of the wall, then we have

$$M(0) = A \times 0^2 + B \times 0x + C = M_{c,Rd} \Longrightarrow C = M_{c,Rd}. \tag{A.3}$$

Moreover, the shear force at maximum bending moment is zero, i.e.,

$$\begin{aligned} \frac{dM}{dx} &= 2Ax + B, \\ \frac{dM}{dx}(0) &= 2A \times 0 + B = 0 \Longrightarrow B = 0. \end{aligned} \tag{A.4}$$

The segment with length $L_E < L$ acts as the simply supported beam such that, in its two ends, the bending moment is zero such that

$$\left(\frac{L_E}{2}\right) = A\times\left(\frac{L_E}{2}\right)^2 + 0\times\frac{L_E}{2} + M_{c,Rd} = 0 \Longrightarrow A = \frac{-4M_{c,Rd}}{L_E^2}. \tag{A.5}$$

Then, (A.2) can simplified into

$$M(x) = M_{c,Rd}\left(1 - \frac{4x^2}{L_E^2}\right). \tag{A.6}$$

The upper and lower supports of the blast wall act as cantilevers such that maximum bending moments of the supports occur at the corners such that

$$\begin{aligned} M(0.5L_E + L_U) &= M_{c,Rd}\left(1 - \frac{4(0.5L_E + L_U)^2}{L_E^2}\right) \\ &= -\left(M_{c,Rd}\right)_U \Longrightarrow \frac{4(0.5L_E + L_U)^2}{L_E^2} \\ &= 1 + \frac{\left(M_{c,Rd}\right)_U}{M_{c,Rd}}, \end{aligned} \tag{A.7}$$

$$\begin{aligned} M(0.5L_E + L_L) &= M_{c,Rd}\left(1 - \frac{4(0.5L_E + L_L)^2}{L_E^2}\right) \\ &= -\left(M_{c,Rd}\right)_L \Longrightarrow \frac{4(0.5L_E + L_L)^2}{L_E^2} \\ &= 1 + \frac{\left(M_{c,Rd}\right)_L}{M_{c,Rd}}. \end{aligned} \tag{A.8}$$

The expressions (A.7) and (A.8) can be simplified into

$$\begin{aligned} L_U &= \frac{L_E}{2}\left(\sqrt{1 + \frac{\left(M_{c,Rd}\right)_U}{M_{c,Rd}}} - 1\right), \\ L_L &= \frac{L_E}{2}\left(\sqrt{1 + \frac{\left(M_{c,Rd}\right)_L}{M_{c,Rd}}} - 1\right). \end{aligned} \tag{A.9}$$

Substituting (A.9) into (A.1), and after simplification, we have equation (7):

$$L_E = \frac{2L}{\sqrt{1 + \left(\left(M_{c,Rd}\right)_U / M_{c,Rd}\right)} + \sqrt{1 + \left(\left(M_{c,Rd}\right)_L / M_{c,Rd}\right)}}. \tag{A.10}$$

B. Rigid-Plastic Beam Model

In rigid plastic type of modelling, the plastic hinge occurs at the middle of the beam where the maximum lateral deflection W_0 will occur (Figure 16).

Obviously, the lateral deformation and velocity pattern will be linear and are given by

$$W = \frac{W_0}{(L/2)}x \Longrightarrow \dot{W} = \frac{W_0}{(L/2)}\dot{x}. \tag{B.1}$$

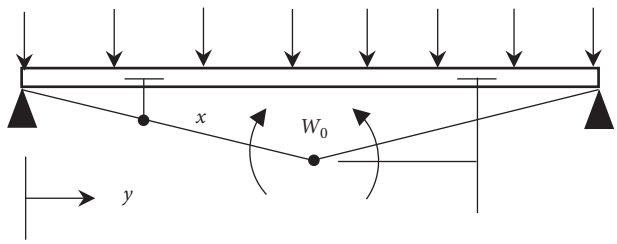

Figure 16: Plastic hinge in the simply supported beam.

Then, considering the form in (B.1), the overall kinetic energy of the beam will be

$$\begin{aligned} \mathrm{KE} &= 2\int_0^L \frac{1}{2}\rho A(\dot{W}(x))^2 dx = \rho A\int_0^L \left(\frac{x}{L/2}\dot{W}_0\right)^2 dx \\ &= \frac{4\rho A\dot{W}_0^2}{L^2}\int_0^{L/2} x^2 dx = \frac{4\rho A\dot{W}_0^2 L^3}{24L^2} = \frac{1}{6}M\dot{W}_0^2. \end{aligned} \tag{B.2}$$

The equivalent mass M_e located at the plastic hinge position should possess the same kinetic energy in (B.2), i.e.,

$$\mathrm{KE} = \frac{1}{2}M_e\dot{W}_0^2. \tag{B.3}$$

Comparing (B.2) with (B.3) will result

$$\frac{1}{2}M_e\dot{W}_0^2 = \frac{1}{6}M\dot{W}_0^2 \Longrightarrow M_e = \frac{1}{3}M. \tag{B.4}$$

Data Availability

The data used to support the findings of this study are available from the corresponding author upon request.

Conflicts of Interest

The author declares no conflicts of interest.

Acknowledgments

The author appreciates Aberdeen University for the time provided to him for doing independent research as part of his duties of an academic post.

References

[1] Fire and Blast Information Group (FABIG), "Design guide for stainless steel blast walls," Technical Note 5, Fire and Blast Information Group Berkshire (UK), Berkshire, UK, 1999.

[2] M. Y. H. Bangash and T. Bangash, *Explosion-Resistant Buildings: Design, Analysis, and Case Studies*, Springer, New York, NY, USA, 2006.

[3] T. Krauthammer, *Modern Protective Structures*, CRC Press, Boca Raton, FL, USA, 2008.

[4] J. Q. Fang, P. Chung, and R. W. Wolfe, "Analysis of a blast-loaded protective wall for bridge columns," *Bridge Structures*, vol. 4, no. 3-4, pp. 135–141, 2008.

[5] L. A. Louca, M. Punjani, and J. E. Harding, "Non-linear analysis of blast walls and stiffened panels subjected to hydrocarbon explosions," *Journal of Constructional Steel Research*, vol. 37, no. 2, pp. 93–113, 1996.

[6] G. K. Schleyer, T. H. Kewaisy, J. W. Wesevich, and G. S. Langdon, "Validated finite element analysis model of blast wall panels under shock pressure loading," *Ships and Offshore Structures*, vol. 1, no. 3, pp. 257–271, 2006.

[7] H. Y. Lei, J. C. Lee, C. B. Lia et al., "Cost–benefit analysis of corrugated blast walls," *Ships and Offshore Structures*, vol. 10, no. 5, pp. 565–574, 2015.

[8] J. M. Biggs, *Introduction to Structural Dynamics*, McGraw-Hill, New York, NY, USA, 1964.

[9] N. M. Newmark, *An Engineering Approach to Blast Resistance Design*, Vol. 121, University of Illinois, Champaign, IL, USA, 1956.

[10] Q. M. Li and H. Meng, "Pulse loading shape effects on pressure-impulse diagram of an elastic-plastic, single-degree-of-freedom structural model," *International Journal of Mechanical Sciences*, vol. 44, no. 9, pp. 1985–1998, 2002.

[11] C. Amadio and C. Bedon, "Viscoelastic spider connectors for the mitigation of cable-supported façades subjected to air blast loading," *Engineering Structures*, vol. 42, pp. 190–200, 2012.

[12] J. Dragos, C. Wu, and K. Vugts, "Pressure-impulse diagrams for an elastic-plastic member under confined blasts," *International Journal of Protective Structures*, vol. 4, no. 2, pp. 143–162, 2013.

[13] A. S. Fallah, E. Nwankwo, and L. A. Louca, "Pressure-impulse diagrams for blast loaded continuous beams based on dimensional analysis," *Journal of Applied Mechanics*, vol. 80, no. 5, article 051011, 2013.

[14] M. H. Hedayati, S. Sriramula, and R. D. Neilson, "Dynamic behaviour of unstiffened stainless steel profiled barrier blast walls," *Ships and Offshore Structures*, vol. 13, no. 4, pp. 403–411, 2018.

[15] M. Aleyaasin, "Protective and blast resistive design of post-tensioned box girders using computational geometry," *Advances in Civil Engineering*, vol. 2018, Article ID 4932987, 7 pages, 2018.

[16] A. C. Van den Berg, "The multi-energy method: a framework for vapour cloud explosion blast prediction," *Journal of Hazardous Materials*, vol. 12, no. 1, pp. 1–10, 1985.

[17] F. D. Alonso, E. G. Ferradás, J. F. S. Pérez, A. M. Aznar, J. R. Gimeno, and J. M. Alonso, "Characteristic overpressure-impulse-distance curves for vapour cloud explosions using the TNO multi-energy model," *Journal of Hazardous Materials*, vol. 137, no. 2, pp. 734–741, 2006.

[18] P. W. Sielicki and M. Stachowski, "Implementation of sapper-blast-module, a rapid prediction software for blast wave properties," *Central European Journal of Energetic Materials*, vol. 12, no. 3, pp. 473–486, 2015.

[19] A. Alia and M. Souli, "High explosive simulation using multi-material formulations," *Applied Thermal Engineering*, vol. 26, no. 10, pp. 1032–1042, 2006.

[20] J. C. Lagarias, J. A. Reeds, M. H. Wright, and P. E. Wright, "Convergence properties of the nelder--mead simplex method in low dimensions," *SIAM Journal on Optimization*, vol. 9, no. 1, pp. 112–147, 1998.

[21] V. R. Feldgun, D. Z. Yankelevsky, and Y. S. Karinski, "A nonlinear SDOF model for blast response simulation of elastic thin rectangular plates," *International Journal of Impact Engineering*, vol. 88, pp. 172–188, 2016.

[22] Y. Ye, L. Zhu, X. Bai, T. X. Yu, Y. Li, and P. J. Tan, "Pressure–impulse diagrams for elastoplastic beams subjected to pulse-pressure loading," *International Journal of Solids and Structures*, vol. 160, pp. 148–157, 2019.

[23] R. Yu, D. Zhang, L. Chen, and H. Yan, "Non-dimensional pressure-impulse diagrams for blast-loaded reinforced concrete beam columns referred to different failure modes," *Advances in Structural Engineering*, vol. 21, no. 14, pp. 2114–2129, 2018.

[24] S. Chen, X. Xing Chen, G. Q. Li, and Y. Lu, "Development of pressure-impulse diagrams for framed PVB-laminated glass windows," *Journal of Structural Engineering*, vol. 145, no. 3, article 04018263, 2019.

[25] A. Khennane, *Introduction to Finite Element Analysis Using MATLAB and ABAQUS*, CRC Press, Boca Raton, FL, USA, 2013.